COMMUNICATION

High Turnover Frequency in the Electrocatalytic Reduction of Nitrous Oxide to Dinitrogen at a Binuclear Copper Complex of 3,5-Diamino-1,2,4-Triazole

Zhengwei Ma,[a] Masaru Kato,*[a,b] Jenny Pirillo,[c] Yuh Hijikata,[d] Takeshi Watanabe,[e] Yohei Uemura,[f] Bang Lu,[g] Satoru Takakusagi,[g] Ken'ichi Kimijima,[h] Hideo Notsu,[i] Ichizo Yagi*[a,b]

[a] Z. W. Ma, Prof. M. Kato, Prof. I. Yagi
Graduate School of Environmental Science, Hokkaido University, N10W5, Kita-ku, Sapporo 060-0810, Japan
[b] Prof. M. Kato, Prof. I. Yagi
Faculty of Environmental Earth Science, Hokkaido University, N10W5, Kita-ku, Sapporo 060-0810, Japan
E-mail: masaru.kato@ees.hokudai.ac.jp; iyagi@ees.hokudai.ac.jp
[c] Dr. J. Pirillo
Faculty of Engineering, Nagoya University, Furumai-cho, Chikusa-ku, Aichi, 464-8603, Japan
[d] Prof. Y. Hijikata
Department of Materials Chemistry, Graduate School of Engineering, Nagoya University, Furumai-cho, Chikusa-ku, Aichi, 464-8603, Japan
[e] Dr. T. Watanabe
Industrial Application and Partnership Division, Japan Synchrotron Radiation Research Institute (JASRI), SPring-8, 1-1-1 Kouto, Sayo 679-5198, Japan
[f] Dr. Yohei Uemura
FXE instrument, European XFEL GmbH, Holzkoppel 4, 22869 Schenefeld, Germany
[g] Dr. Bang Lu, Prof. Satoru Takakusagi
Institute for Catalysis, Hokkaido University N21 W10, Sapporo 001-0021, Japan
[h] Dr. Ken'ichi Kimijima
Photon Factory, Institute of Materials Structure Science, High Energy Accelerator Research Organization, 1-1 Oho, Tsukuba, Ibaraki, 305-0801, Japan
[i] Dr. Hideo Notsu
Department of Materials Science and Engineering, Institute of Science Tokyo, S8-26 , 2-12-1 Ookayama Meguro-ku 152-8550, Japan

Supporting information for this article is given via a link at the end of the document.

Abstract: Nitrous oxide (N_2O) is a potent greenhouse gas and an ozone-depleting substance. Electrocatalytic N_2O reduction (e-N_2ORR) is a promising approach to remove N_2O from the air under ambient conditions. However, developing noble-metal-free e-N_2ORR electrocatalysts with high Faradaic efficiency (FE) and turnover frequency (TOF) remains a challenge because of the weak binding of N_2O and the high kinetic barrier for deoxygenation reaction. In this work, inspired by the multinuclear copper active site of nitrous oxide reductases, a binuclear copper complex of 3,5-diamino-1,2,4-triazole supported on carbon black of Ketjenblack (CuHdatrz/KB) was utilized for the e-N_2ORR at pH 13 and 298 K. CuHdatrz/KB achieves a high FE of ≈100% at -0.3 V vs. RHE for the e-N_2ORR to N_2 and TOF up to ≈700 h^{-1}, which is one–two orders of magnitude higher than those of the previously reported molecular-based catalysts. *In situ* X-ray absorption spectroscopy confirmed that Cu(II) ions of CuHdatrz/KB are reduced to Cu(I) keeping the binuclear core, suggesting that the multinuclear copper active sites is crucial to efficiently catalyze the e-N_2ORR like the nitrous oxide reductase.

Excess nitrous oxide (N_2O) from anthropogenic sources disrupts natural denitrification processes (NO_3^-→NO_2^-→NO→N_2O→N_2),[1,2] leading to a gradual increase in atmospheric N_2O levels.[3] As of June 2024, the atmospheric N_2O concentration reached 338 ppb, rising by approximately 1 ppb annually.[4] N_2O has a global warming potential ~300 times higher than that of CO_2 on a per-mass basis and is a persistent ozone-depleting substance.[5,6] Without intervention, this trend will worsen.[7] Therefore, it is crucial to minimize N_2O emission and explore effective methods to convert N_2O into N_2. N_2O removal technologies have been developed including thermal decomposition systems, photocatalytic systems, and electrocatalytic systems.[8–13] Although thermal decomposition efficiently removes N_2O, the high cost associated with continuous energy input limits its widespread application.[14,15] Photocatalytic systems suffer from wide band gaps and rapid charge recombination, significantly limiting their efficiency and scalability, even with advanced modifications such as doping and material coupling.[16,17]

The electrocatalytic N_2O reduction reaction (e-N_2ORR) offers a low-energy, efficient, and scalable alternative to thermal decomposition and photocatalysis for converting N_2O into N_2 or NH_3 under ambient conditions. Palladium-based electrocatalysts are particularly effective for the e-N_2ORR to N_2, with a Tafel slope of 84 ± 7 mV dec^{-1} in 0.1 M NaOH, suggesting potential for further performance enhancement.[18] Therefore, strategies such as microstructure modification or alloying have been widely explored.[2,11,19,20] Notably, our previous work highlighted that combining palladium with platinum and tin can enhance N_2O

adsorption, suppress hydrogen adsorption, and boost e-N_2ORR activity at palladium-tin interfaces.[2] Nevertheless, palladium's scarcity and cost limit its scalability.

Non-noble metal-based electrocatalysts offer a cost-effective and abundant alternative to noble metal catalysts. However, these catalysts face inherent challenges that limit their performance and adoption. In addition to the inherent difficulty of N_2O adsorption on metals, attributed to its poor σ-donating and π-accepting characteristics, these catalysts must overcome the high dissociation energy of the N-O bond and competitive adsorption from hydrogen.[21,22]

Biological insights into nitrous oxide reductases provide valuable inspiration for designing advanced electrocatalysts that address the challenges faced by non-noble metal systems. In nature, many bacteria contain nitrous oxide reductases, which are a multi-copper metalloenzyme and catalyze the reduction of N_2O to N_2 and H_2O using two electrons and two protons, making this process highly attractive.[23,24] There are two copper sites in nitrous oxide reductase **(Figure S3)**: the internal electron transfer site, Cu_A, and the enzymatic active site, Cu_Z (the Cu_4S cluster).[24] The Cu_A site receives electrons from cytochrome *c* or cupredoxin and transfers them to the Cu_Z site, at which N_2O is adsorbed and then reduced. In this process, a sulfide bridging ligand of Cu_Z delocalizes electrons over the multi-copper active site, and overcomes the high kinetic barrier for N-O cleavage.[25] Structural mimics of the Cu_Z site have been reported.[26–28] For example, a mononuclear copper(II) complex of (2,6-bis(bis-2-*N*-methylimidazolyl)phosphino)pyridine, Cu-MeIm$_4$P$_2$Py, has been reported for the e-N_2ORR,[29] where mimicking the ligand structure of the reaction center of the nitrous oxide reductase exhibits high e-N_2ORR activity with a turnover frequency (TOF) of 54 h^{-1} and a Faradaic efficiency (FE) of 83%.These findings motivated us to study a multinuclear copper complex as a functional mimic of the nitrous oxide reductase.

In this study, we investigated the e-N_2ORR activity of a copper complex of 3,5-diamino-1,2,4-triazole (CuHdatrz) in alkaline media. CuHdatrz features the binuclear copper center and is prepared via a one-step process. Electrochemical measurements of CuHdatrz supported on carbon black of Ketjenblack (CuHdatrz/KB) under N_2O revealed high e-N_2ORR activity and selectivity. *In situ* X-ray absorption spectroscopy measurements of CuHdatrz/KB revealed the change of the oxidation state of the metal center and binuclear core structure of CuHdatrz/KB under electrochemical conditions. To elucidate the high e-N_2ORR activity of CuHdatrz/KB, pH-dependence of the onset potential for the e-N_2ORR and density functional theory (DFT) calculations of its reduced form were also investigated.

CuHdatrz/KB was prepared following a previously reported procedure (**Figure 1a**).[30] KB, $CuSO_4{\cdot}5H_2O$, and Hdatrz were mixed in Milli-Q water under ultrasonication, and then stirred overnight at RT. The resulting product was collected under vacuum filtration and then dried under vacuum to obtain CuHdatrz/KB. A ligand of Hdatrz links the two Cu ions. High-angle annular dark field-scanning transmission electron microscopy (HAADF-STEM) images show bright white spots, indicating that Cu atoms are uniformly distributed on the KB surface **(Figure 1c)**. This observation is further supported by energy dispersive X-ray spectroscopy (EDS) mapping, where the uniform distribution of N and Cu atoms **(Figure 1d)**. The EDS result (**Figure S4**) confirms an N to Cu atomic ratio of 5:1, demonstrating that CuHdatrz was successfully synthesized and anchored onto the KB surface.

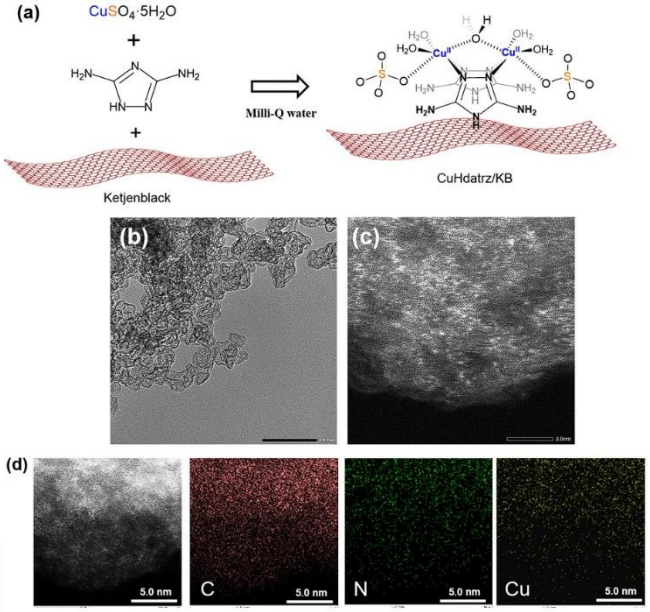

Figure 1. (a) The synthesis process of CuHdatrz/KB; (b) TEM and (c) HAADF-STEM and EDS mapping images of CuHdatrz/KB.

Cyclic voltammograms (CVs) of CuHdatrz/KB display the potential-dependence of the competition of the e-N_2ORR and hydrogen evolution reaction (HER). CVs in Britton-Robinson (BR) buffered aqueous solutions under Ar (**Figure S5**) confirmed that CuHdatrz/KB shows the electrocatalytic activity for the HER. In the presence of N_2O, the onset potential shifted in the positive direction, along with the increase in the current density, resulting from the e-N_2ORR by CuHdatrz/KB (**Figure S5**). As the pH increases, the gap between onset potentials and current densities for the HER and e-N_2ORR becomes more pronounced. As shown in **Figure 2a**, the gap between onset potentials for the e-N_2ORR and HER is approximately 0.12 V at pH 2. When the pH increases to 7 and 13, the potential gaps increase to 0.31 and 0.58 V, respectively. The current density differences follow a similar trend, being lowest at pH 2 (1.39 mA cm^{-2}), increasing at pH 7 (2.31 mA cm^{-2}), and reaching its highest value at pH 13 (3.02 mA cm^{-2}) at -0.6 V vs. RHE. These results indicate that the e-N_2ORR becomes more dominant at pH 13 than the HER, justifying subsequent investigations under this condition.

CuHdatrz/KB shows its high FE for the e-N_2ORR (**Figure 2c**). FE was determined from chronoamperometry and gas chromatography. For chronoamperometry measurements, a series of potentials (-0.2, -0.3, -0.4, -0.5, and -0.6 V vs. RHE) were applied individually to the working electrode (**Figure S6**), and the generated gases were analyzed using an online gas chromatograph. Throughout the catalytic process for 1 h, the current remained stable at each applied potential, demonstrating high stability of CuHdatrz/KB. N_2 was the primary product with the FE for N_2 approaching 100% at potentials ≥ -0.3 V vs. RHE (**Figure S7c**). At ≤ -0.4 V vs. RHE, the e-N_2ORR competes with the HER and FE for N_2 decreases as the potential decreases: 95% FE for N_2 at -0.4 V; 85% at -0.5 V, and 67% at -0.6 V vs.

RHE. In contrast, the FE for H_2 steadily increases: 5.1% at -0.4 V; 17% at -0.5 V; and 33% at -0.6 V vs. RHE. Thus, both the HER and e-N_2ORR occur simultaneously, and the HER dominates the electrocatalytic process at negative potentials.[31] Note that FE for NH_3 is <1% (**Figure S8**) and therefore the main product for the e-N_2ORR is N_2.

CuHdatrz/KB exhibited the highest TOF among reported molecular electrocatalysts. TOFs were determined based on the redox-active copper ions determined from CVs of CuHdatrz/KB under Ar (~0.64 μmol cm^{-2}, which is 95% of the total loading metal ions) (**Figure 2b**): 108 h^{-1} at −0.2 V; 110 h^{-1} at −0.3 V; 294 h^{-1} at −0.4 V; 405 h^{-1} at −0.5 V; 656 h^{-1} at −0.6 V vs. RHE (**Figure 2d**). Compared to previously reported TOFs for molecular-based catalysts, CuHdatrz exhibited the highest TOF (**Figure 2e** and **Table S1**).[29,32–36] For example, the copper(II) complex of Cu-MeIm$_4$P$_2$Py achieved a TOF of 54 h^{-1} (**Figure 2e**).[29] This complex has the single Cu(II) center,[28] implying that the binuclear copper center in CuHdatrz is more effective in catalyzing N_2O reduction. Other metal complexes exhibited TOFs ranging from 3.9 to 476 h^{-1}: a nickel complex of 1,4,8,12-tetra-azacyclopenta (Ni-[15]aneN$_4$);[32] a ruthenium complex of 2,6-bis(diisopropylphosphino)pyridine (Ru-N(SiMe$_2$CH$_2$PtBu$_2$));[33] a rhodium-platinum complex of multidentate phosphine olefin (Rh-Pt-olefin);[34] a rhenium complex of bipyridyl carbonyl (Re-bpy));[35] an iridium complex of 2-[(Mesitylimidazol-2-ylidene)(di-tert-butyl)phosphino]pyridine (Ir-MesCNP);[36] an iron complex of tetraphenylporphyrin (Fe-TPP)[37] (**Figure 2e**). Although cobalt complexes of bis(tetra-aminophthalocyanine) (Co-Clam)[38] and of tetra-amino-phthalocyanine (Co-TAPc)[39] were also reported to exhibit high selectivity and activity for the e-N_2ORR, their TOFs were not provided. The comparison in TOFs between these metal complexes indicates that designing and developing metal complexes with high N_2O reduction activity under ambient conditions remains challenging. Moreover, the TOF of CuHdatrz/KB approaches the range of the natural nitrous oxide reductase enzymes, which achieves TOFs between 63 and 1171 h^{-1}.[40,41]

CuHdatrz/KB exhibited high stability for the e-N_2ORR. It maintained a stable current at -0.3 V vs. RHE over 24 h, the four 6 h periods. Almost 100% FE remained even after this long-term experiment and the total turnover number reached to 2656 after 24 h (**Figure S9**). Inductively coupled plasma optical emission spectrometry measurements of the catalyst film and electrolyte solution confirmed that ~98% of the initial copper ions remained after the long-term experiment. Furthermore, almost no change was observed in X-ray photoelectron spectroscopy profiles of CuHdatrz/KB before and after the long-term experiment (**Figure S10**). Thus, CuHdatrz/KB is highly durable for the e-N_2ORR. Note that the stability of the catalyst film highly depends on the type of binder used: about 30% current loss was observed in CVs under N_2O after 100 cycles with Nafion whereas an almost negligible decay was observed with polyvinylidene difluoride (**Figure S11**),[42] which was used for the product analysis and long-term experiments.

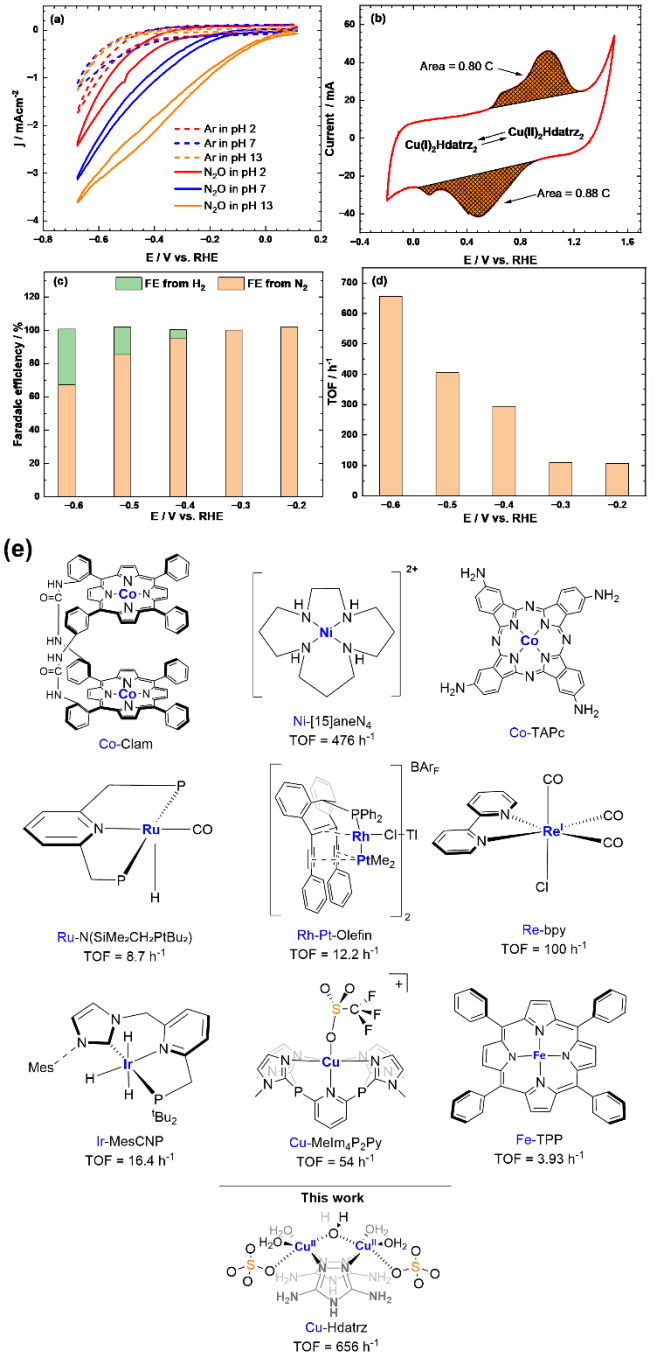

Figure 2. (a) CV_S of CuHdatrz/KB in BR buffer solutions at pH 2 (red), pH 7 (blue), and pH 13 (orange) under Ar (dot line) and N_2O (solid line) range from -0.675 to 0.125 V vs. RHE, Scan Rate =10 mV s^{-1}, (b) and in under Ar from -0.2 to 1.5 V vs. RHE (pH 13, Scan Rate = 10 mV s^{-1}). (c) FEs and (d) TOFs for N_2 at -0.6, -0.5, -0.4, -0.3 and -0.2 V vs. RHE in pH 13, (e) structures and TOFs for the N_2O reduction of Co-Clam[38], Ni-[15]aneN$_4$,[32] Co-TAPc,[39] Ru-N(SiMe$_2$CH$_2$PtBu$_2$),[33] Rh-Pt-Olefin,[34] Re-bpy,[35] Ir-MesCNP,[36] Cu-MeIm$_4$P$_2$Py,[29] and Fe-TPP[37].

An *ex situ* X-ray absorption spectrum of CuHdatrz/KB in the Cu K-edge X-ray absorption near edge structure (XANES) region was recorded to understand the initial oxidation state of the Cu center. As shown in **Figure 3a**, the *ex situ* XANES spectrum of CuHdatrz closely aligns with that of CuO, confirming the presence

of the Cu(II) ion in its initial state. This result is consistent with the result of single-crystal X-ray analysis.[43] The potential-dependent XANES spectra of CuHdatrz/KB show that Cu(II)Hdatrz is directly converted into a single reduced Cu(I) species under electrochemical conditions without any decomposition: in other words, $Cu^{II/I}$ transformation is reversible (**Figure S12**).[30] These results suggested that the reduction of Cu(II) to Cu(I) species for CuHdatrz is the initial step for the e-N_2ORR.

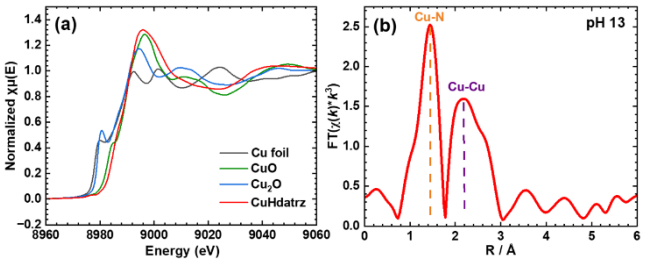

Figure 3. (a) Cu *K*-edge XANES spectra of CuHdatrz and reference samples (Cu foil, CuO, and Cu_2O), (b) FT-EXAFS oscillation of CuHdatrz at 0.12 V vs. RHE at pH 13.

In situ Cu *K*-edge X-ray absorption spectroscopy of CuHdatrz/KB was performed at pH 13 and then Fourier transforms of extended X-ray absorption fine structure (FT-EXAFS) oscillations were analyzed (**Figure 3b**). The FT-EXAFS analysis reveals two distinct peaks assigned to Cu-N and Cu-Cu paths in Cu(I)Hdatrz, highlighting the retention of the binuclear copper structure post-reduction. The curve-fitting analysis of the FT-EXAFS data provides further details on coordination numbers and bond distances: a coordination number of 1.5 and a bond length of 1.85 ± 0.01 Å for the Cu-N path and a coordination number of 0.5 and a bond length of 2.59 ± 0.01 Å for the Cu-Cu path (**Table S2**), showing a significantly shorter Cu-Cu distance compared to that for CuHdatrz before reduction (3.49 Å).[43] In typical Cu(I) complexes, intramolecular Cu-Cu bond distances range from 2.38 to 2.71 Å,[44] confirming the presence of the binuclear copper unit of Cu(I)Hdatrz even under reductive conditions. Notably, in nitrous oxide reductase, interaction with N_2O induces structural changes in the Cu_Z center, adjusting the Cu-Cu distances to enhance N_2O adsorption and facilitate electron transfer.[45] Furthermore, in synthetic Cu_Z models, reduction leads to the Cu_Z center adopting a more square geometry with decreasing the distance between $1Cu_Z$ and $4Cu_Z$, responsible for N_2O adsorption, from 3.0 to 2.8 Å.[46] These results collectively highlight the critical role of multinuclear structures, where the dynamic adjustment of metal-metal distances is essential for facilitating catalytic processes. The change in oxidation states of the binuclear Cu center of CuHdatrz, along with the alteration in Cu-Cu distance, resembles the nitrous oxide reductase.

The catalytic behavior of CuHdatrz/KB is strongly influenced by pH. As shown in **Figure 4a**, in the pH range of 7-10, the slope is 5.9 mV per pH, which is equivalent to -53 mV per pH relative to a pH-independent potential (**Figure S13**), closely aligning with the Nernstian prediction of -59 mV per pH.[30] This suggests that the rate-determining step involves the transfer of the same number of electron(s) and proton(s): two electrons and two protons or one electron and one proton. Since the binuclear Cu(II) active site is reduced to Cu(I) during the catalytic process, the rate-determining step is more likely to involve the transfer of two electrons and two protons.[30,47] In strong alkaline media at pH 10-14, the onset potential no longer exhibits a linear dependence on pH (**Figure 4a** and **Figure S13**). This change reflects a change in the reaction mechanism for the e-N_2ORR catalyzed by CuHdatrz, which can be induced by alkaline environments at pH 10-14. It is most likely that deprotonation from ligands contributes to this change.

EXAFS oscillation profiles of Cu-Hdatrz at different pH provide insights into changes of the local atomic environment in CuHdatrz.[48] The EXAFS oscillation profiles at around 2 $Å^{-1}$ show nearly identical oscillations at pH 7 and pH 10, whereas those at pH 13 differ significantly (**Figure 4b-d**). Differences in the FT-EXAFS spectra (**Figure S14)** and curve-fitting analysis (**Table S2**) at various applied potentials further illustrate these structural changes. Possibly, the ligand deprotonation occurs at pH 13, altering the electronic structure of CuHdatrz. In DFT calculations, we obtained optimized structures of deprotonated forms with Cu(I) ions and hydroxide ligands (**Figure S15**), further supporting that the deprotonation from H_2O ligands is more favorable than that of Hdatrz ligands. These results suggest that designing ligands for the multinuclear copper active sites is critical to facilitate the efficient e-N_2ORR catalysis and deprotonation of ligands plays a critical role in modulating the activity of CuHdatrz for the e-N_2ORR.

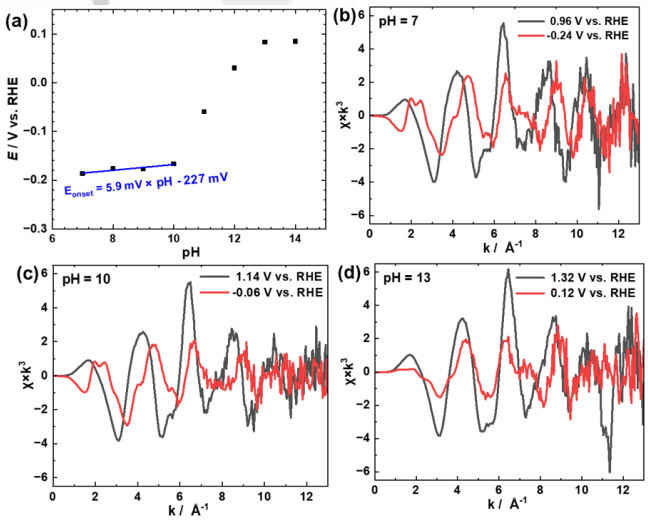

Figure 4. (a) Plots of onset potential for the e-N_2ORR vs. pH. The plots gave a linear relationship with $E_{onset\ vs.\ RHE}$ = 5.9 mV × pH - 227 mV in pH 7-10; EXAFS oscillations of Cu-Hdatrz under nitrogen at (b) pH 7, (c) pH 10, and (d) pH 13.

In conclusions, we demonstrated the e-N_2ORR activity of the binuclear copper CuHdatrz/KB under ambient conditions. CuHdatrz/KB achieved the 100% FE with the TOF of 110 h^{-1} at -0.3 V vs. RHE and pH 13. Even at -0.5 V vs. RHE, showing 85% FE with a TOF of 405 h^{-1}. These high FEs and TOFs surpass previously reported molecular electrocatalysts for the e-N_2ORR. *In situ* X-ray absorption spectroscopy of CuHdatrz/KB revealed that Cu(II) is reduced to Cu(I) and the binuclear copper core remains after the reduction. The high e-N_2ORR activity of CuHdatrz/KB especially under strongly alkaline (pH 10–14) conditions can be induced by structural changes of CuHdatrz involving the deprotonation of H_2O molecules, supported by DFT

calculations. Our results demonstrate that multinuclear Cu active sites in CuHdatrz/KB are critical for efficient e-N_2ORR and illustrate the feasibility of mimicking nitrous oxide reductases with Cu-based molecular catalysts. Notably, TOFs of natural nitrous oxide reductases (~29,400 h^{-1} with artificial electron mediators)[49] remain far superior to CuHdatrz/KB, highlighting the need for further efforts to develop functionally mimicking Cu-based molecular catalysts with high e-N_2ORR activity.

Supporting Information

The authors have cited additional references within the Supporting Information.

Acknowledgements

The authors thank Takashi Tanioka (Faculty of Engineering, Hokkaido University) for taking the HAADF-STEM and EDS mapping images. This work was supported by EXEX doctoral fellowship, JFE 21st Century Foundation, JSPS KAKENHI (Grant numbers 19H02664 and 21K05124), "Advanced Research Infrastructure for Materials and Nanotechnology (ARIM)" programs of MEXT for Hokkaido University (JPMXP1222HK0033, JPMXP1223HK0012, JPMXP1224HK0036 and JPMXP1225HK0022) and Molecular Science (Grant number JPMXP09S18MS0029). Synchrotron radiation experiments were performed at the BL14B2 of SPring-8 with the approval of the Japan Synchrotron Radiation Research Institute (JASRI) (Proposal nos. 2023A1791 and 2023B1916) and at the BL12C of Photon Factory, KEK (Proposal nos. 2010G200, 2013G173, 2015G103, and 2016G671).

Keywords: Electrocatalysis • N_2O reduction • Denitrification • N_2O reductase • metalloenzyme mimic

[1] M. Hu, Z. Yu, T. J. Griffis, W. H. Yang, J. Mohn, D. B. Millet, J. M. Baker, D. Wang, *Environ Sci Technol* **2024**, *58*, 9701-9713.

[2] A. C. Sarker, M. Kato, M. Kawamura, T. Watanabe, I. Yagi, *Catal Sci Technol* **2024**, *14*, 4137-4141.

[3] O. Badr, S. D. Probert, *Appl Energy* **1992**, *41*, 177–200.

[4] Global Monitoring Laboratory, "Trends in Atmospheric Nitrous Oxide (N_2O)", can be found under https://gml.noaa.gov/ccgg/trends_n2o, **2024**.

[5] D. Uraguchi, Y. Ueki, T. Ooi, *Science* 2009, *326*, 120-123.

[6] X. Wu, J. Du, Y. Gao, H. Wang, C. Zhang, R. Zhang, H. He, G. Lu, Z. Wu, *Chem Soc Rev* **2024**, *53*, 8379-8423.

[7] M. Konsolakis, *ACS Catal* **2015**, *5*, 5701-5716.

[8] J. G. Yun, J. Y. Kim, H. M. Lee, G. Y. Baik, M. K. Jeon, J. H. Yun, J. G. Hong, *ACS Omega* **2022**, *7*, 3434-3441.

[9] S. Fu, Q. Song, Q. Yao, *Energy Fuels* **2015**, *293*, 1695-1702.

[10] B. H. Ko, B. Hasa, H. Shin, Y. Zhao, F. Jiao, *J Am Chem Soc* **2022**, *144*, 1258-1266.

[11] K. Kim, J. Byun, H. Kim, K. S. Lee, H. S. Lee, J. Kim, T. Hyeon, J. J. Kim, J. W. Han, *ACS Catal* **2021**, *11*, 15089-15097.

[12] S. Atri, S. Uma, R. Nagarajan, M. Gregor, T. Roch, M. Filip Edelmannova, M. Reli, K. Koci, M. Motola, O. Monfort, *Energy Advances* **2024**, *3*, 1956-1964.

[13] O. Delaunay, A. Denicourt-Nowicki, A. Roucoux, *J Phys Chem Solids* **2024**, *194,* 112242.

[14] M. Jabłońska, R. Palkovits, *Catal Sci Technol* **2016**, *6*, 7671–7687.

[15] M. Galle, D. W. Agar, O. Watzenberger, *Chem Eng Sci* **2001**, *56*, 1587-1595.

[16] R. J. Stella, I. Sreevani, T. R. Gurugubelli, R. V. S. S. N. Ravikumar, R. Koutavarapu, *Catalysts* **2023**, *13*, 1312.

[17] K. Kočí, M. Reli, I. Troppová, M. Šihor, J. Kupková, P. Kustrowski, P. Praus, *Appl Surf Sci* **2017**, *396*, 1685-1695.

[18] A. Aziznia, A. Bonakdarpour, E. L. Gyenge, C. W. Oloman, *Electrochim Acta* **2011**, *56*, 5238-5244.

[19] A. C. Sarker, M. Kato, I. Yagi, *Electrochim Acta* **2022**, *425*, 140628.

[20] M. Kato, J. Zheng, Y. Deng, F. Saito, Y. Unuma, S. Oka, K. Tamura, I. Yagi, *ACS Catal* **2025**, *15*, 7710–7719.

[21] K. Severin, *Chem Soc Rev* **2015**, *44*, 6375-6386.

[22] Y. Wang, W. Zhou, R. Jia, Y. Yu, B. Zhang, *Angewandte Chemie* **2020**, *132*, 5388–5392.

[23] E. M. Johnston, C. Carreira, S. Dell'Acqua, S. G. Dey, S. R. Pauleta, I. Moura, E. I. Solomon, *J Am Chem Soc* **2017**, *139*, 4462-4476.

[24] J. M. Chan, J. A. Bollinger, C. L. Grewell, D. M. Dooley, *J Am Chem Soc* **2004**, *126*, 3030-3031.

[25] S. J. Gorelsky, S. Ghosh, E. I. Solomon, *J Am Chem Soc* 2006, *128*, 278-290.

[26] S. C. Rathnayaka, N. P. Mankad, *Coord Chem Rev* 2021, *429*, 213718.

[27] B. J. Johnson, W. E. Antholine, S. V. Lindeman, N. P. Mankad, *Chem Commun* **2015**, *51*, 11860-11863.

[28] B. J. Johnson, S. V. Lindeman, N. P. Mankad, *Inorg Chem* **2014**, *53*, 10611-10619.

[29] J. L. Martinez, J. E. Schneider, S. W. Anferov, J. S. Anderson, *ACS Catal* **2023**, *13*, 12673-12680.

[30] M. Kato, K. Kimijima, M. Shibata, H. Notsu, K. Ogino, K. Inokuma, N. Ohta, H. Uehara, Y. Uemura, N. Oyaizu, T. Ohba, S. Takakusagi, K. Asakura, I. Yagi, *Phys Chem Chem Phys* **2015**, *17*, 8638-8641.

[31] A. Kudo, A. Mine, *J Electroanal Chem* **1996**, *408*, 267-269.

[32] I. Taniguchi, T. Shimpuku, K. Yamashita, H. Ohtaki, *J Chem Soc Chem Commun* **1990**, *13*, 936-938.

[33] R. Zeng, M. Feller, Y. Ben-David, D. Milstein, *J Am Chem Soc* **2017**, *139*, 5720-5723.

[34] P. Jurt, A. S. Abels, J. J. Gamboa-Carballo, I. Fernández, G. Le Corre, M. Aebli, M. G. Baker, F. Eiler, F. Müller, M. Wörle, R. Verel, S. Gauthier, M. Trincado, T. L. Gianetti, H. Grützmacher, *Angew Chem Int Ed* **2021**, *60*, 25372-25380.

[35] R. Deeba, F. Molton, S. Chardon-Noblat, C. Costentin, *ACS Catal* **2021**, *11*, 6099-6103.

[36] I. Ortega-Lepe, P. Sánchez, L. L. Santos, P. Lara, N. Rendón, J. López-Serrano, V. Salazar-Pereda, E. Álvarez, M. Paneque, A. Suárez, *Inorg Chem* **2022**, *61*, 18590-18600.

[37] J. S. Stanley, X. S. Wang, J. Y. Yang, *ACS Catal* **2023**, *13*, 12617-12622.

[38] J. P. Collman, M. Marrocco, C. M. Elliott, M. L'Her, *J Electroanal Chem* **1981**, *124*, 113-131.

[39] J. Zhang, Y.-H. Tse, A. B. P. Lever, W. J. Pietro, *J Porphyrins Phthalocyanines* **1997**, *1*, 323-331.

[40] B. C. Berks, D. Baratta, D. J. Richardson, S. J. Ferguson, *Eur J Biochem* **1993**, *212*, 467-476.

[41] S. Dell'Acqua, S. R. Pauleta, E. Monzani, A. S. Pereira, L. Casella, J. J. G. Moura, I. Moura, *Biochemistry* **2008**, *47*, 10852-10862.

[42] U. O. Nwabara, A. D. Hernandez, D. A. Henckel, X. Chen, E. R. Cofell, M. P. de-Heer, S. Verma, A. A. Gewirth, P. J. A. Kenis, *ACS Appl Energy Mater* **2021**, *4*, 5175–5186.

[43] E. Aznar, S. Ferrer, J. Borrás, F. Lloret, M. Liu-González, H. Rodríguez-Prieto, S. García-Granda, *Eur J Inorg Chem* **2006**, 5115–5125.

[44] M. A. Carvajal, S. Alvarez, J. J. Novoa, *Chem Eur* J, **2004**, *10*, 2117-2132.

[45] A. Pomowski, W. G. Zumft, P. M. H. Kroneck, O. Einsle, *Nature* **2011**, *477*, 234–237.

[46] B. J. Johnson, W. E. Antholine, S. V. Lindeman, M. J. Graham, N. P. Mankad, *J Am Chem Soc* **2016**, *138*, 13107-13110.

[47] M. S. Thorum, J. Yadav, A. A. Gewirth, *Angew Chem Int Ed* **2009**, *48*, 165-167.

[48] F. D'acapito, *Introduction to Ab-Initio Methods for EXAFS Data Analysis*, **2007**.

[49] S. Wan, Y. Mottiar, A. M. Johnson, K. Goto, I. Altosaar, *Transgenic Res* **2012**, *21*, 593-603.

Entry for the Table of Contents

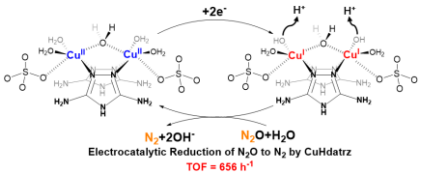

Inspired by nitrous oxide reductase, a binuclear copper complex supported by carbon black was utilized for the electrocatalytic N_2O reduction under ambient conditions. The binuclear Cu center enables exceptionally high turnover frequency and nearly 100% Faradaic efficiency for the electrochemical N_2O reduction.